Available online at www.sciencedirect.com
SCIENCE DIRECT®
Journal of Non-Crystalline Solids 351 (2005) 3075–3080
JOURNAL OF NON-CRYSTALLINE SOLIDS
www.elsevier.com/locate/jnoncrysol

Effect of B, Si and Cr on the mechanical properties of Fe-based amorphous metallic ribbons

I.A. Figueroa [a], I. Betancourt [b], G. Lara [b], J.A. Verduzco [a,*]

[a] Instituto de Investigaciones Metalúrgicas (UMSNH) Ed. 'U', C.U., P.O. Box 888, Morelia, Michoacan 58000, Mexico
[b] Instituto de Investigaciones en Materiales (UNAM), P.O. Box 70-360, Mexico D.F. 04510, Mexico

Received 21 September 2004; received in revised form 12 July 2005
Available online 24 August 2005

Abstract

In this work, we present a systematic study about the effect of B and Si content on the mechanical properties of three melt spun amorphous alloy series: $Fe_{92-x}Si_8B_x$ ($10 \leqslant x \leqslant 18$) – series 1, $Fe_{90-x}Si_{10}B_x$ ($10 \leqslant x \leqslant 18$) – series 2 and $Fe_{82-x}Si_{10}B_xCr_8$ ($12 \leqslant x \leqslant 20$) – series 3. The Vickers microhardness increased as the B content was increased for all the series. On the other hand, the fracture strength, σ_{TS}, for series 1 exhibited a gradual increase as a function of B contents. In contrast, σ_{ST} showed maximum values for series 2 and 3 at concentrations of 14 and 16 at.% B, respectively. In general, it was observed that the microhardness and strength of the alloy series with 8 at.% Si was higher compared with 10 at.% Si series. Studies of fractography by SEM revealed two types of fracture for the ribbons subjected to tensile tests: ductile for alloys with low B contents ($\leqslant$14 at.%) and brittle for both, alloys with high B contents ($\geqslant$16 at.%) and Cr-containing alloys. These variations of fracture type are used to explain the observed tendency for microhardness and tensile strength as a function of B content.

PACS: 61.43.Dq; 62.20.Mk; 62.20.−x

1. Introduction

It is widely established that amorphous metallic alloys (ribbons and wires) have excellent mechanical strength, especially for Fe-based compositions [1]. Likewise, it has also been reported that metalloid elements have an important influence on metallic glasses affecting their thermal stability and mechanical properties [2]. For instance, Si and B are the metalloid elements more used to obtaining metallic glasses because they enhance the glass forming ability. On the other hand, it has been reported that relatively high content of Si (10 at.%) in FeCrSiB alloy wires increase their mechanical strength [3]. In contrast, a subsequent investigation [4] stated that some Fe-based amorphous wires with relatively low Si content (7.5 at.%) and high B (15 at.%) concentration have better mechanical properties. These contradictory results motivated this present study on the mechanical properties of FeSiB amorphous ribbons with variable metalloid concentration, with the aim of contributing for the clarification of these results.

2. Experimental

Three alloy composition series were studied: Series 1, with the general formula $Fe_{92-x}Si_8B_x$ ($10 \leqslant x \leqslant 18$); series 2, $Fe_{90-x}Si_{10}B_x$ ($10 \leqslant x \leqslant 18$) and series 3, $Fe_{82-x}Si_{10}B_xCr_8$ ($12 \leqslant x \leqslant 20$) ($\Delta x = 2$). High purity elements (Fe 99.9%, Si 99.99%, Cr 99.9% and B 99.99%) were

* Corresponding author. Tel./fax: +52 443 316 7414.
E-mail address: verduzco@zeus.umich.mx (J.A. Verduzco).

0022-3093/$ - see front matter © 2005 Elsevier B.V. All rights reserved.
doi:10.1016/j.jnoncrysol.2005.07.017

used to obtain master ingots of 10 g for each composition by means of Ti-gettered arc-melting in Ar atmosphere. Metallic ribbons of each composition were produced using the chill block melt spinning technique into a sealed chamber under He atmosphere at a roll speed of 40 m s^{-1}.

The alloy ribbons microstructure was analyzed using a Siemens D5000 diffractometer with Cu Kα radiation at 40 kV and 20 mA. The scanning range in the analysis was from 5° to 85°. The material was classified as amorphous if the diffraction pattern presented the typical liquid-like structure, characteristic of an amorphous phase. Further confirmation of the amorphous microstructure was realised by means of a high resolution transmission electronic microscope (HRTEM) FEG-PHILIPS TECNAI F20 operated at 200 kV. Vickers microhardness measurements were carried out with a digital Lietz–Wetzlar microhardmeter using a load of 50 g for 20 s. A minimum of 20 readings per sample were taken to obtain an average. Ten samples of 0.05 m long of each alloy were prepared for bending tests. Ribbons that showed the ability to be bent 180° without fracture were classified as flexible. Tensile strength measurements were carried out at deformation rates of $1.6E-4\ s^{-1}$ using an Instron 1125 universal testing machine. The bent and tensile fractured ribbons morphologies were observed in a scanning electron microscope JEOL JSM-6400 operated at 20 kV.

3. Results

3.1. Microstructure

X-rays diffractograms of all alloy ribbon series presented an amorphous structure (see Fig. 1). Fig. 2 shows an HRTEM image together with its diffraction pattern (calculated from Fourier transformation) corresponding to a $Fe_{80}Si_{10}B_{10}$ alloy, which is similar to alloys containing B contents lower than 16 at.%. A liquid-like structure is manifested with no evidence of nanocrystals. In addition, the diffraction pattern shows concentric circles characteristic of a non-crystalline structure. However, for alloys containing 16 at.% B or higher, some crystalline zones were observed (Fig. 3).

3.2. Mechanical properties

3.2.1. Bending

Table 1 displays the bending test results. The whole series 1 ($Fe_{92-x}Si_8B_x$) showed a flexible behavior while series 2 ($Fe_{90-x}Si_{10}B_x$) and series 3 ($Fe_{92-x}Cr_8Si_8B_x$) exhibited flexible behavior until 16 at.% B. Beyond this B content, alloy ribbons manifest brittle behavior.

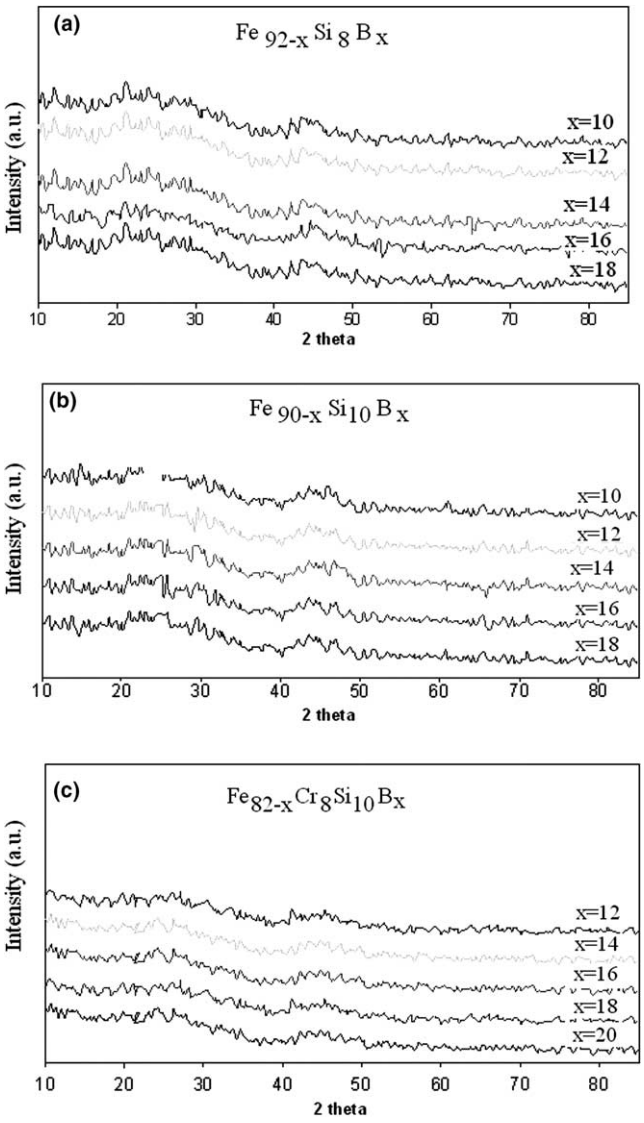

Fig. 1. X-ray diffraction patterns for all alloy ribbons studied. (a) series 1, (b) series 2 and (c) series 3.

3.2.2. Microhardness

Fig. 4 shows the Vickers microhardness results, H_v, as a function of B for the three alloys series. Series 1 exhibited higher H_v values than series 2 and 3 for B contents up to 18 at.%. For instance, H_v for series 1 varied from 9.12 to 12.01 GPa, while the values for series 2 ranges from 8.41 to 11.96 GPa and series 3 from 9.7 to 12.42 GPa, for 20 at.% B. It is observed a gradual enhancement of H_v with the increment of B content, but the series with less Si content showed higher values than those with higher contents of this element.

3.2.3. Tensile strength

Fig. 5 shows the tensile strength, σ_{TS}, as a function of B concentration for all the alloy series. Alloys with 8 at.% Si content possess higher σ_{TS} than those containing 10 at.% Si. However, it can be appreciated that series

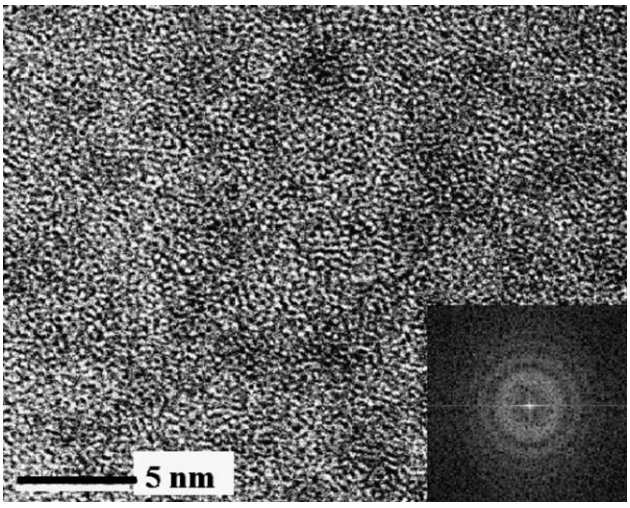

Fig. 2. HRTEM image and diffraction pattern (calculated from Fourier transformation) of a $Fe_{80}Si_{10}B_{10}$ amorphous alloy ribbon.

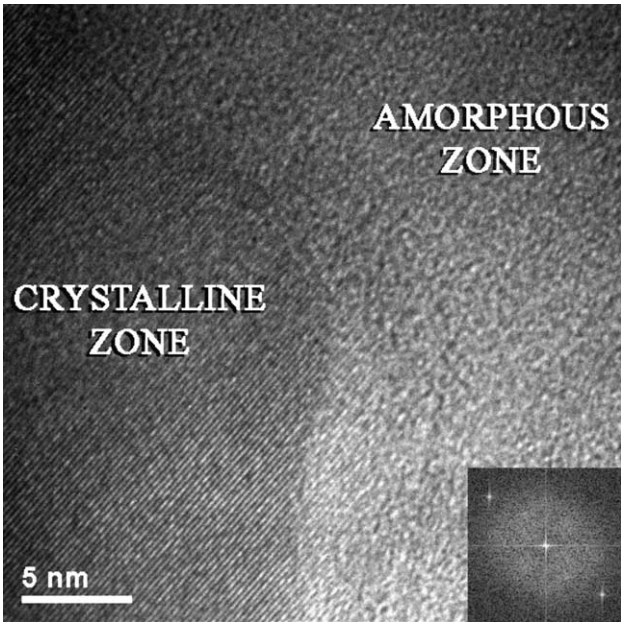

Fig. 3. HRTEM image and diffraction pattern (calculated from Fourier transformation) of a $Fe_{64}Cr_8Si_{10}B_{18}$ amorphous alloy ribbon.

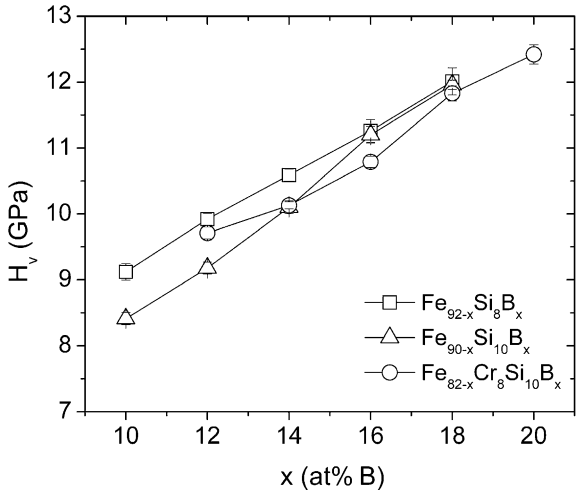

Fig. 4. Vickers microhardness as a function of B content for all the alloy series. Connecting lines are for eye guidance only.

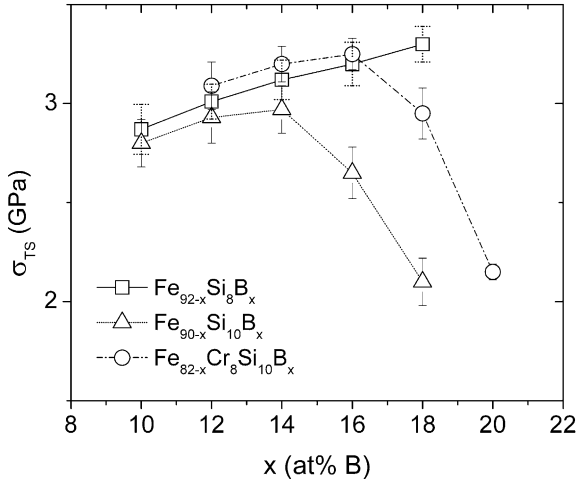

Fig. 5. Tensile strength as a function of B content all the alloy series. Connecting lines are for eye guidance only.

2 has a maximum resistance at 14 at.% B, dropping drastically beyond this B content. On the other hand, the maximum resistance of series 3 was reached at 16 at.% B, with a diminishing tendency for higher B concentration. σ_T for series 1 showed lineal increment behavior within the range 2.87–3.30 GPa. On the other hand, σ_{TS} values for series 2 were higher in the three first alloys up to a value of 2.97 GPa ($Fe_{76}Si_{10}B_{14}$), and then decreased significantly to a value of 2.10 GPa ($Fe_{72}Si_{10}B_{18}$).

Table 1
Ductile/brittle behavior determined from 180 bent test for all the alloy series

Series 1		Series 2		Series 3	
Composition	State	Composition	State	Composition	State
$Fe_{82}Si_8B_{10}$	Flexible	$Fe_{80}Si_{10}B_{10}$	Flexible	$Fe_{70}Cr_8Si_{10}B_{12}$	Flexible
$Fe_{80}Si_8B_{12}$	Flexible	$Fe_{78}Si_{10}B_{12}$	Flexible	$Fe_{68}Cr_8Si_{10}B_{14}$	Flexible
$Fe_{78}Si_8B_{14}$	Flexible	$Fe_{76}Si_{10}B_{14}$	Flexible	$Fe_{66}Cr_8Si_{10}B_{16}$	Brittle
$Fe_{76}Si_8B_{16}$	Flexible	$Fe_{74}Si_{10}B_{16}$	Brittle	$Fe_{64}Cr_8Si_{10}B_{18}$	Brittle
$Fe_{74}Si_8B_{18}$	Flexible	$Fe_{72}Si_{10}B_{18}$	Brittle	$Fe_{62}Cr_8Si_{10}B_{20}$	Brittle

Series 3 showed the same behavior that series 2, showing a maximum σ_{TS} value of 3.25 GPa ($Fe_{66}Cr_8Si_{10}B_{16}$) and a minimum value of 2.15 GPa ($Fe_{62}Cr_8Si_{10}B_{20}$).

3.3. Fractography

3.3.1. Bending

A SEM image for a flexible $Fe_{74}Si_8B_{18}$ alloy ribbon is displayed in Fig. 6. The alloy showed plastic deformation with heterogeneous and localized flow together with intense shear bands. Such morphologies are similar to those reported previously in amorphous wires [5].

3.3.2. Tensile fracture

Two different types of tensile fractures were observed by SEM, one was ductile (Fig. 7), corresponding to a $Fe_{76}Si_8B_{16}$ amorphous alloy ribbon; and the other was brittle (Fig. 8), corresponding to a $Fe_{62}Cr_8Si_{10}B_{20}$ alloy. No necking was observed along the tensile axis close to the fractures for both cases.

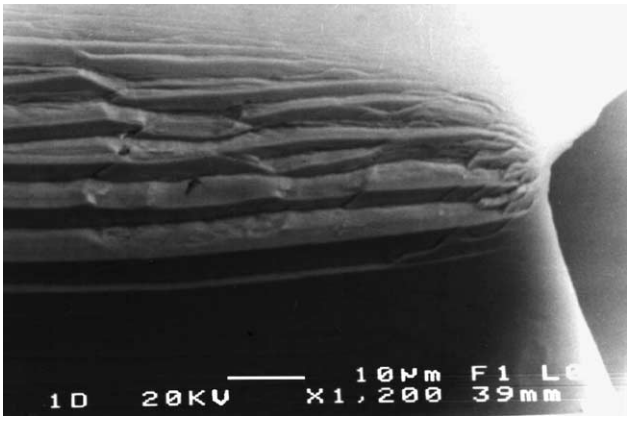

Fig. 6. SEM image of a $Fe_{74}Si_8B_{18}$ alloy ribbon bent tested. The plastic deformation is manifested as shear bands.

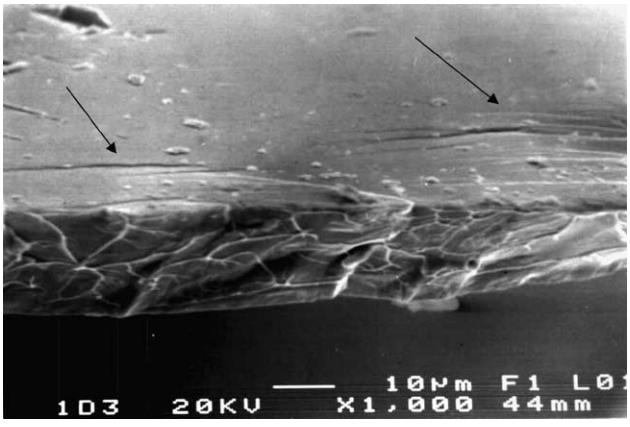

Fig. 7. Ductile tensile fracture surface of an $Fe_{76}Si_8B_{16}$ amorphous alloy ribbon, where the even (A) and veined zones (B) are observed. Arrows indicate shear bands.

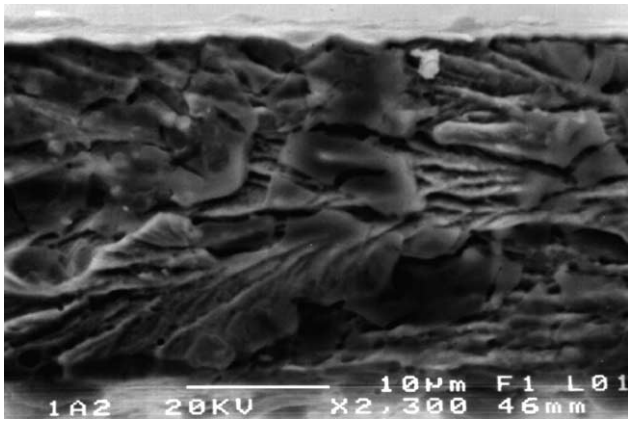

Fig. 8. Brittle tensile fracture surface of an $Fe_{62}Cr_8Si_{10}B_{20}$ amorphous alloy ribbon.

4. Discussion

4.1. Mechanical properties

4.1.1. Bending

The flexibility of all alloys of series 1 can be ascribed to the relative low amount of Si, since the increment of this element up to 10 at.% (series 2 and 3) resulted in a brittle behavior for B concentrations beyond 16 at.%. The embrittlement of series 3 was more significant, because only the $Fe_{70}Cr_8Si_{10}B_{12}$ and $Fe_{68}Cr_8Si_{10}B_{14}$ alloys were flexible. This behavior can be attributed to the onset of crystallization, as it is evidenced in Fig. 3. Similar behavior observed in $Fe_{77.5-x}Cr_xSi_{7.5}B_{15}$ alloys was attributed to self-annealing during casting [3]. In addition, Olofinjana and Davies [3] reported that it was difficult to cast flexible wires with amorphous structures with contents of Cr $\geqslant$ 8 at.% because the relative high Cr-metalloid concentration is strongly related to the brittleness as a consequence of an ultra-fine segregation due to a short range diffusive migration between the atomic species during the cast.

4.1.2. Microhardness

It has been reported that the microhardness of metallic glasses is strongly influenced by the average concentration of s and d electrons per metallic transition atom (e/a) [6]. Specifically, microhardness increases with decreasing e/a (e/a decreases with the substitution of Cr for Fe in FeCrSiB alloys). In the present study, such theory can be applied (for the case of series 3 only) because the Fe content decreases by adding B, and hence, less electrons to the electronic concentration are expected. From this, e/a values were calculated according to the following equation [7]:

$$e/a = \frac{[\text{at.\%Fe}(s+d)_{\text{Fe}}] + [\text{at.\%Cr}(s+d)_{\text{Cr}}]}{\text{at.\%Fe} + \text{at.\%Cr}} \quad (1)$$

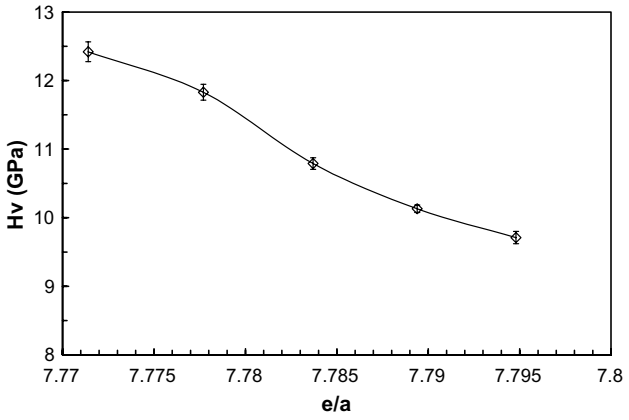

Fig. 9. Vickers microhardness plotted against the average outer electrons ($s+d$) concentration of metallic atoms (e/a) for the $Fe_{82-x}Cr_8Si_{10}B_x$ melt spun alloys. Connecting lines are for eye guidance only.

where $(s+d)_{Fe}$ is 8 and $(s+d)_{Cr}$ is 6. Fig. 9 shows H_v as a function of e/a for the $Fe_{62}Cr_8Si_{10}B_{20}$ alloy. A decreasing trend is manifested with increasing e/a values, confirming the H_v (e/a) dependence reported in [6]. For the remaining Cr-free alloy series, this analysis does not apply, because e/a is 8 in all the cases, since Fe is the only transition element that provides electrons.

4.1.3. Tensile strength

The tensile resistance decrements can be explained on the basis of ribbon brittleness as indicated in Table 1. It can also be assumed an increasing directionality of interatomic forces, which may result in a change in the atomic bond from metallic to covalent [8]. For the present work, the effect of Si on the mechanical properties of FeBSi amorphous alloys resulted in a different sense compared with results reported in [3] for alloy wires, but it is in agreement with those reported recently in amorphous wires [4] and ribbons [7] as well of similar compositions, where it is established that alloys with 7.5 at.% Si and 15 at.% B contents showed higher σ_{TS} values than for alloys having 10 at.% Si and 12 at.% B. This behavior can be associated to the tendency of a short range ordering [9], resulted from an enhanced glass forming ability, which in turn leads to a stronger atomic interaction between Fe atoms and metalloids [3,10]. In addition, the smaller B atomic size (compared with Si) also plays a significant role in occupying more efficiently the intersticies formed in the dense packed model for amorphous microstructure proposed by Bernal [11], which makes the material denser and stronger. On the other hand, the enhanced σ_{TS} values obtained for series 3 at $x = 12$, 14 and 16 can be attributed to the Fe substitution for Cr. In this sense, Hagiwara et al. [2] found that σ_{TS} increased with replacing Fe with small quantities of another transition metal, M, in the order of M = Cr, V, Mo, W and Nb, which was attributed to an increment in the bond forces between metal–metalloid in $(Fe–M)_{75}Si_{10}B_{15}$ amorphous alloys. It was also found that M increases the glass forming ability of the alloy because of the strong nature of chemistry bond between metalloids and solute metal.

4.2. Fractography

4.2.1. Bending

The shear bands resulted by bending were formed rapidly at the beginning of deformation. It has been reported [12] that the deformation of the deep and large shear bands should give rise to compositional disordering during high stress deformation or through an increase in the average atomic volume. In this case, the orientation of the shear band is parallel to the direction of the stress bending load.

4.2.2. Tensile fracture

The absence of necks along the tensile axis close to fractures may be considered as an evidence of localized deformation on surfaces of the shear bands. The regions observed on ductile fracture surfaces have been explained as follows [5]. Most of tensile fractures of amorphous ribbon and wires occur on shear bands involving inhomogeneous flow, followed by initiation and propagation of a crack and finally by a viscous flow, exhibiting two distinctive morphology zones: one uniform and the other veined. Most of fractures occurred at angles of 45° to the tensile axis, which may demonstrate that the fracture was also shear induced for the present study. On the other hand, the alloys presented as brittle in Table 1 showed fractures of such type, less common to this class of materials, having an uneven surface fracture. In this case, the deformation was not induced over a shear plane of 45° (Fig. 8). It can be observed that the fracture started in two opposite planes. This type of brittle fracture is attributed to the high Cr and B contents. Fig. 8 also shows that the fracture planes are approximately normal to the tensile axis. It has been proposed [13] that brittle fracture of metallic glasses is due to a process of cleavage, which occurs when a stress concentrator (cluster, partial crystallinity as indicated in Fig. 3, microcrack, microsegregation or any particle harder than the matrix) is subjected to a tensile stress affording to reach the theoretical fracture stress of the material before the plastic flow stops or traps the crack propagation, which relaxes the stress. It is worth to notice that this type of fracture has been characterized to be ductile [14] which contrasts with Fig. 7 of the present work.

5. Conclusions

The effect of variable Si and B content on the mechanical properties of FeBSi amorphous ribbons

has been established. Vickers microhardness increased with increasing B content for all the alloys series. The fracture strength for series 1 increased gradually as a function of B content, while σ_{TS} for series 2 and 3 reached maximum values at 14 at.% and 16 at.% B concentrations, respectively. It was found that the mechanical properties of the alloy series with 8 at.% Si were superior compared with the series with 10 at.% Si. These results confirm a similar tendency observed in amorphous wires of same composition [4].

Acknowledgments

J.A. Verduzco acknowledges the financial support received from CONACyT and the Universidad Michoacana de San Nicolás de Hidalgo, by projects I39169-U and 1.21, respectively. I. Betancourt is grateful for financial support provided by project IN1196033, UNAM and for technical support provided by A. Maciel and E. Sanchez.

References

[1] L.A. Davis, S.K. Das, J.C.M. Li, M.S. Zedalis, Int. J. Rapid Solidif. 8 (1994) 73.
[2] M. Hagiwara, A. Inoue, T. Masumoto, Metall. Trans. 13A (1982) 373.
[3] A.O. Olofinjana, H.A. Davies, Mater. Sci. Eng. A 186 (1994) 143.
[4] R. Torres, J.A. Verduzco, Mater. Manuf. Processes 18 (1) (2003) 79.
[5] A.O. Olofinjana, H.A. Davies, Int. J. Rapid Solidif. 8 (1994) 225.
[6] T. Masumoto, Sci. Rep. RITU. 26 (4&5) (1983) 246.
[7] J.A. Verduzco, J.I. Betancourt, F. Saavedra, E. Reynoso, J. Non-Cryst. Solids 329 (2003) 163.
[8] H.S. Chen, Rep. Progr. Phys. 43 (4) (1980) 353.
[9] A. Inoue, H.S. Chen, J.T. Krause, T. Masumoto, M. Hagiwara, J. Mater. Sci. 18 (1983) 2743.
[10] M. Hagiwara, A. Inoue, T. Masumoto, The critical thickness for the formations of Fe-, Ni-, and Co-based amorphous alloys with metalloids, Science Report Research Institutes, Tohoku University, 29, 1981, p. 351.
[11] J.D. Bernal, Nature 183 (1959) 141.
[12] D.E. Polk, D. Turnbull, Acta Metall. 20 (1972) 493.
[13] F. Spaepen, A.I. Taub, Flow and fracture, in: F.E. Luborsky (Ed.), Amorphous Metallic Alloys, Butterworths, London, 1983, p. 231.
[14] Y.C. Niu, X.F. Bian, W.M. Wang, J. Non-Cryst. Solids 341 (2004) 40.